Influence of Ba^{2+} consumption and intermediate dwelling during processing of $YBa_2Cu_3O_7$ nanocomposite films

Hannes Rijckaert[1] **Jens Hänisch**[2] **Glenn Pollefeyt**[1] **Michael Bäcker**[3] **Isabel Van Driessche**[1]

[1]Department of Chemistry, SCRiPTS, Ghent University, Ghent, Belgium

[2]Institute for Technical Physics, Karlsruhe Institute of Technology, Eggenstein Leopoldshafen, Germany

[3]Deutsche Nanoschicht GmbH, Rheinbach, Germany

Correspondence
Isabel Van Driessche, Department of Chemistry, SCRiPTS, Ghent University, Ghent, Belgium.
Email: Isabel.VanDriessche@UGent.be

Abstract

Achieving high-critical current densities (J_c) with small artificial pinning centers is a crucial challenge for $YBa_2Cu_3O_{7-\delta}$ (YBCO) nanocomposite thin films fabricated using chemical solution deposition methods. In this work, the YBCO texture, structure purity, and its J_c properties were improved by understanding the influence of preformed ZrO_2 nanocrystals (Ba^{2+} consumption) during the nucleation and growth mechanism. This comprehensive study leads to an additional intermediate dwelling step during thermal process to increase the YBCO nuclei density before the YBCO growth, resulting to a self-field J_c of 5-6 MA/cm^2 at 77 K for undoped and ZrO_2-doped YBCO films. Counter-intuitively, the space and size distribution of the ZrO_2 nanocrystals in the YBCO matrix are independent of this intermediate dwelling step.

KEYWORDS

chemical solution deposition, low fluorine YBCO, nanocomposite, nanoparticles, vortex pinning

1 INTRODUCTION

The successful and reliable growth of biaxially textured $YBa_2Cu_3O_{7-\delta}$ (YBCO) nanocomposite films with high in-field current carrying capability on flexible metallic substrates is essential for its use for electric power devices as well as high-field magnets. Regarding this, there is considerable interest in improving the critical current density (J_c) and its anisotropy in applied magnetic fields. Several groups have been busy with the quest for the best manufacturing method to grow epitaxial YBCO films on a textured or polycrystalline template of one or more oxide buffer layers on a metallic substrate.[1,2] To date, superconductive-YBCO films are often deposited through physical and chemical deposition processes such as pulsed laser deposition, electron beam evaporation and metal-organic chemical vapor deposition (MOCVD) to meet the practical requirements for commercialization. Use of the pulsed laser deposition process has resulted in some of the thickest (>4 μm) and highest J_c doped-YBCO films (>4 MA/cm^2 at 77 K, self-field) deposited on CeO_2-buffered Y-stabilized ZrO_2 templates,[3] while MOCVD starting from trifluoroacetate (TFA)-based precursors shows to be a good competitor with J_c of 3 MA/cm^2 (at 77 K, self-field) at a thickness of 2.2 μm for 20 mol-% Zr-doped $(Gd,Y)Ba_2Cu_3O_{7-\delta}$ films deposited on Hastelloy substrates with biaxially textured MgO templates and a $LaMnO_3$ cap layer.[4] However, the physical deposition processes require high vacuum and result in higher production costs in contrast to, for example MOCVD which only requires a moderate vacuum.[1–5] Chemical solution deposition (CSD) technology offers an economically viable synthesis route toward low-cost medium performance as it operates under normal pressure.[5–8] The CSD technique is a highly flexible method for the fabrication of oxide thin films, however, it is not straightforward to tailor its epitaxial growth of desired microstructure.

Besides the established CSD approach starting from the trifluoroacetate metal-organic decomposition (TFA-MOD) method,[9] which is based on the ex-situ BaF_2 process,[10] several research groups have already reported on a more

benign modified TFA-MOD method, that is, using low-fluorine (LF)[11–13] and even fluorine-free solutions.[14] Obtaining good superconducting performances of the undoped and nanodoped YBCO film in function of the applied magnetic field and the direction of this field remain a challenge. These performances can be improved by the incorporation of preformed nanocrystals or nano-sized secondary phases as artificial pinning centers in YBCO matrix as they can act pinning centers for the vortices.[15,16] Currently, some research has already investigated on the link between the influence of preformed nanocrystals and its surface chemistry with the final YBCO properties. It has been discovered that preformed nanocrystals can lead to better pinning properties while a choice of ligands is very crucial to obtain good YBCO properties.[17–19] Nevertheless, understanding of nucleation and growth mechanism of undoped and nanodoped YBCO films during the CSD process of TFA-MOD methods should be essential to improve the superconducting properties. These mechanisms are already been described in literature, but it is still unknown what the influence of the preformed nanocrystals is on the nucleation and growth mechanism. While pulsed laser deposition is already an advanced research method to elucidate the effects of nano-sized secondary phases on the pinning landscape in high-temperature superconducting films,[20–22] there is limited knowledge of the control over the formation of nano-sized secondary phases during nucleation and growth step of CSD-YBCO methods. In previous research,[18] it was seen that the addition of single metal oxide nanocrystals (eg, ZrO_2) leads to the formation of double metal oxide nanocrystals (eg, $BaZrO_3$) due to its Ba^{2+} consumption. This latter has a negative effect on the formation of (002)-oriented BaF_2 superstructure, which acts as good template for nucleation and growth of YBCO nanocomposite film.

In this work, we present a comprehensive study to elucidate the mechanism of the LF-YBCO nucleation and the influence of single metal nanocrystal addition herein, by the introduction of an intermediate heating step at several temperatures preceding the YBCO crystallization at 800°C. This comprehensive study shows the possibilities to improve the functional and structural properties of epitaxial thin films in several material classes through refinement of the thermal processing.

2 EXPERIMENTAL DETAILS

2.1 Preparation and CSD of YBCO precursor solution

$YBa_2Cu_3O_{7-\delta}$ precursor solutions with a 66% reduction in fluorine content were prepared by dissolving Y-propionate, Ba-TFA, and Cu-propionate in an Y:Ba:Cu ratio of 1:2:3 in methanol. Small 3-5 nm cubic ZrO_2 nanocrystals (distorted tetragonal crystal structure[17]) in toluene were synthesized and purified according to De Keukeleere et al.[23] To transfer these as-synthesized nanocrystals to polar solvents (eg, methanol), a ligand exchange with a phosphonate-containing copolymer was introduced, according to Rijckaert et al.[17] These copolymer-stabilized nanocrystals were finally added to the highly ionic YBCO precursor solution,[24] resulting in ZrO_2-doped YBCO precursors solutions. Both precursor solutions have a total metal concentration of 1.08 mol/L. The (100) $LaAlO_3$ substrates were spin-coated with 2000 rpm for 2 minutes and subsequently pyrolyzed by heating to 400°C with a heating rate of 3-5°C/min in a wet oxygen atmosphere. After the pyrolysis, the microstructure consists of CuO nanoparticles embedded in an amorphous matrix of $Ba_{1-x}Y_xF_{2-x}$ (BYF). The pyrolyzed YBCO films were subsequently processed to obtain the desired superconducting film with a high-temperature thermal treatment at 800°C for 70 minutes in a humid 100 ppm O_2 in N_2 atmosphere with or without an intermediate dwelling step. When such an intermediate dwelling step is introduced, the pyrolyzed YBCO films were heated with a rate of 5°C/min to the dwell temperatures of 600, 650, or 700°C, respectively, and kept for 45 minutes in a humid 100 ppm O_2 in N_2 atmosphere plus 15 minutes in a dry 100 ppm O_2 in N_2 atmosphere. After this additional dwelling step, the samples were fast heated to 800°C (15°C/min) under dry conditions and switched back to humid conditions at 770°C before it reaches 800°C to avoid the formation of a/b grains. The inlet gas was bubbled through a water bath with a temperature of 23°C. After this crystallization step, the flowing atmosphere was switched to dry O_2 at 450°C for 2 hours during the annealing step to convert the tetragonal YBCO phase to the superconducting orthorhombic phase.

2.2 Characterization of the thin layers

The growth morphology and structure of the undoped and ZrO_2-doped YBCO films were examined by means of X-ray diffraction (XRD) on a Bruker D4 diffractometer (Cu K_α). The distribution of metal ions was determined via Time-Of-Flight (TOF) Secondary Ion Mass Spectrometry (SIMS) using a modified TOF-SIMS IV from ION-TOF GmbH, equipped with a 25 kV Bi LMIG and 10 kV C_{60} sputter source (see supplemental materials for more details).

Scanning electron microscopy (SEM) images were obtained using a FEI Nova 600 Nanolab Dual Beam FIB-SEM (FEI, Eindhoven, Netherlands) where the thickness was estimated from cross-sectional SEM images. High-resolution and high-angle annular dark-field scanning transmission electron microscopy (HRTEM and HAADF-

STEM) images were taken on a JEOL JEM-2200FS TEM (JEOL, Tokyo, Japan) with a Cs corrector, operated at 200 kV. Chemical information was obtained via the combination of HAADF-STEM (*Z*-contrast) and phase analysis via energy dispersive X-ray spectroscopy. For HAADF-STEM analysis, a cross-sectional lamella was obtained using ion milling techniques via the FIB *in situ* lift-out procedure with an Omniprobe™ (Ted Pella Inc., Redding, CA) extraction needle and top cleaning.

The self-field critical current density J_c at 77 K was determined inductively with a 50 μV voltage criterion in a Cryoscan™ system (THEVA GmbH, Ismaning, Germany). In-field transport J_c in maximum Lorentz force configuration was determined in 4-probe geometry on 40-50 μm wide and 800 μm long laser-cut bridges at magnetic fields up to 9 T with an electric field criterion of 1 μV/cm in Quantum Design Physical Property Measurements System.

3 RESULTS AND DISCUSSION

The nucleation and growth of TFA-based or reduced fluorine-based YBCO systems can be found in literature[25–27] and is described as the *ex situ* BaF_2 process.[10–27] Generally, it is reported that the formation of BaF_2 instead of $BaCO_3$ occurs when a fluorine content of more than 15.4% is used.[28] In this *ex situ* BaF_2 process, the BYF phase formed after the pyrolysis transforms into $Ba(O,F)_2$ and Y_2O_3 composites while Y_2O_3 reacts with CuO nanoparticles to form $Y_2Cu_2O_5$ which is followed by the nucleation of the tetragonal $YBa_2Cu_3O_6$ ($YBCO_6$) phase at temperatures between 650 and 700°C. However, the accumulation of preformed nanocrystals on the $LaAlO_3$ interface must be avoided during the pyrolysis because it can result in worse epitaxial growth of YBCO.[18] In this work, a homogeneous distribution of the ZrO_2 nanocrystals throughout the layer is observed, and no accumulation of ZrO_2 nanocrystals on the $LaAlO_3$ interface can be observed in the pyrolyzed films as confirmed via TOF-SIMS analysis (Figure S1A). The use of a copolymer as stabilization ligand leads to a spread-out of nanocrystals in the pyrolyzed matrix because of good nanocrystal surface chemistry.[17] This spread-out of nanocrystals is a very important step to avoid the tendency to accumulations of nanocrystals during the growth.

Here, in order to study the nucleation and growth process of YBCO films, pyrolyzed samples with smooth and crack-free surfaces were crystallized and quenched by quickly pulling them out of the tube furnace at several intermediate temperatures (400, 500, 600, 650, 700, 750, and 800°C). After XRD analysis on these samples, the XRD pattern of the YBCO layer (Figure 1A) starting from LF-YBCO precursors shows that BYF reflections (111) ($2\theta = 24.9°$), (002) ($2\theta = 28.8°$), and (202) ($2\theta = 42.2°$) shift toward lower 2θ angles for increasing temperature. This is due to a compositional change and related to the development of a BaF_2-based superstructure, which has been found to provide a good template for YBCO nucleation.[29] Upon increasing the temperature, Y is removed from the BYF phase to form Y_2O_3 (400) ($2\theta = 33.7°$) which reacts with fine nanoparticles of CuO ($11\underline{1}$) ($2\theta = 35.5°$) to form a submicron-sized $Y_2Cu_2O_5$ phase (peaks at $2\theta = 33.4$) at ~650°C. Similar to the results published in literature, the reaction between CuO and Y_2O_3 is almost directly followed the nucleation of $YBCO_6$. The following intermediate reactions during the nucleation mechanism are shown in Equations 1 and 2. The first trace content of $YBCO_6$ nucleation can be identified at 650°C using the YBCO (005) reflection ($2\theta = 38.3°$). To clarify the influence of the addition of ZrO_2 nanocrystals, with the purpose to use them as pinning centers, on the nucleation and growth of YBCO, quenched ZrO_2-doped YBCO films were also synthesized and analyzed via XRD (Figure 1B). From these results, it is shown that the formation of the (002)-oriented BaF_2 superstructure is reduced to temperatures between 650 and 700°C compared to undoped YBCO. This can most likely be assigned to the reaction between the BYF phase and ZrO_2 nanocrystals, resulting in the formation of $BaZrO_3$ particles. These particles cannot be observed in XRD, probably due to the combination of small quantity, small size and homogeneous distribution in the YBCO matrix as confirmed via TEM analysis of ZrO_2-doped YBCO films (Figure 3A). Above 700°C, the BaF_2 phase is reduced due to the reaction with the $Y_2Cu_2O_5$ phase to the final $YBCO_6$ phase. This observation corresponds to literature data[17,18–30] and shows the reactivity of single metal oxide nanocrystals during the nucleation and growth of YBCO film.

$$2\ CuO + Y_2O_3 \rightarrow Y_2Cu_2O_5 \tag{1}$$

$$Y_2Cu_2O_5 + 2\ Ba(O,F)_2 + 4CuO \underset{H_2O}{\rightarrow} 2\ YBa_2Cu_3O_{7-x} + 4\ HF \tag{2}$$

The addition of ZrO_2 nanocrystals results indeed in a decreased content of the BaF_2 structure (Figure 1D) which could degrade the epitaxial growth of YBCO. This results in a deviation of the growth mechanism, changing the intermediate products that are formed. The presence of intermediate products has been estimated from the intensity of the XRD reflections of BaF_2 (111) and YBCO (005), from experiments using different quench temperatures as shown in Figure 1C,D. We can conclude that ZrO_2-doped YBCO films exhibit a different evolution of BaF_2 (111) compared to undoped YBCO. Also with increasing temperature, the intensity of the YBCO (005) peak increases although the ZrO_2-doped YBCO seems to display some

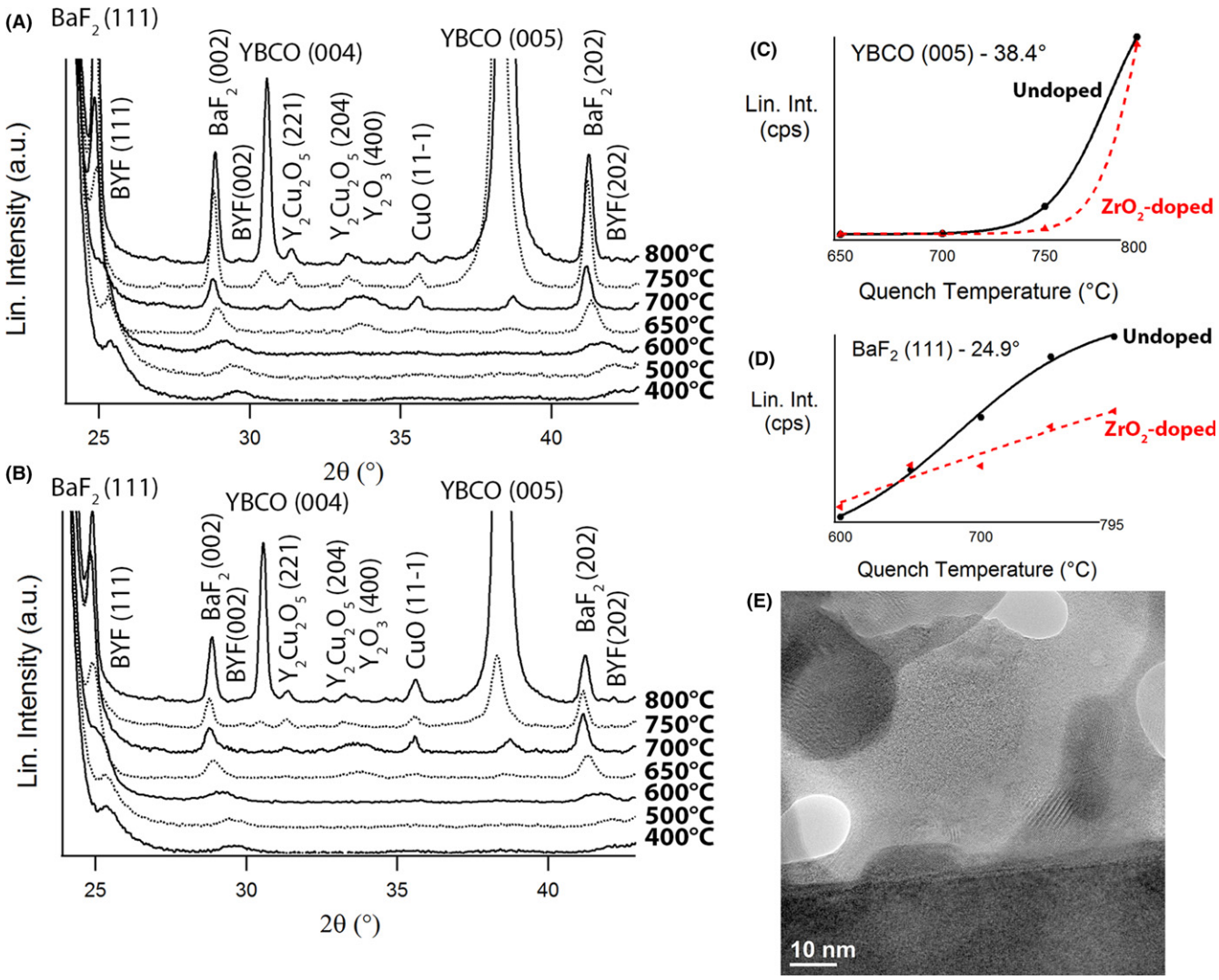

FIGURE 1 X ray diffraction (XRD) scans of (A) undoped and (B) ZrO_2 doped $YBa_2Cu_3O_{7-\delta}$ (YBCO) films quenched at various intermediate temperatures. Temperature dependence of the intensity of XRD peaks of (C) YBCO (005) ($2\theta = 38.4°$) and (D) BaF_2 (111) ($2\theta = 24.9°$). (E) A High resolution transmission electron microscopy image of ZrO_2 doped YBCO film quenched at 650°C [Color figure can be viewed at wileyonlinelibrary.com]

delay in the YBCO nucleation mechanism. It is also remarkable that the intensity of fine CuO (11$\underline{1}$) nanoparticles for YBCO with nanocrystals is higher than for YBCO without nanocrystals. As the ZrO_2 nanocrystals react with the BaF_2 structure before they react with $Y_2Cu_2O_5$, this reactivity of ZrO_2 nanocrystals will enhance the feasibility of the hetero-epitaxial growth of large and agglomerated $BaZrO_3$ particles on the $LaAlO_3$ interface during growth of YBCO nanocomposite films. However, from Figure 1C,D as well as from the absence of a $BaZrO_3$ (200) reflection in Figure 1B, an accumulation and formation of $BaZrO_3$ at the $LaAlO_3$ interface can be ruled out during the nucleation and growth process in this work. It is also confirmed via HRTEM image of the quenched sample at 650°C (Figure 1E), where no accumulation of ZrO_2 nanocrystals can be observed. Therefore, these results prove that the reactivity of ZrO_2 nanocrystals is unrelated to the worse epitaxial YBCO growth but instead related to delayed reaction and growth of the YBCO structure due to the smaller content of Ba^{2+} during the nucleation.

As concluded from the quench study (Figure 1), Ba^{2+} reacts with ZrO_2 nanocrystals to $BaZrO_3$ particles in the temperature range between 650 and 700°C and the nucleation of YBCO occurs at ~650°C. In order to promote the nucleation of YBCO, we have introduced an intermediate heat treatment step at temperatures of 600, 650, and 700°C with a dwell time of 1 hour with 45′ wet and 15′ dry 100 ppm O_2 in N_2 atmosphere, as proposed by Chen et al.[12] Whereas YBCO grains start growing at 700°C as indicated by the YBCO (005) peak from the XRD data (Figure 2) of the quenched samples after dwelling for 1 hour, they remain small and only increase in nuclei density at

650°C broader peak of YBCO (005) , indicating an increased amount of small nucleation sites. However, a difference in the intensity of YBCO (005) peaks (Figure 2) of undoped and ZrO_2-doped YBCO films after dwelling at 650°C can be observed, indicating that the presence of nanocrystals during the thermal process also affects the nucleation mechanism. When dwelling at 600°C, no YBCO (005) was observed for both undoped and ZrO_2-doped samples while some reduction in the BaF_2 reflection is observed because of their reactivity with ZrO_2 nanocrystals. Thus, the addition of nanocrystals in the YBCO matrix is not destructive for the YBCO growth despite the reactivity of the single metal oxide nanocrystals. The addition of these nanocrystals only changes the nucleation kinetics and thermodynamics of the YBCO phase.

To confirm that the higher amount of nucleation sites (caused by the additional dwelling step) leads to the improved properties, the pyrolyzed samples undergo full crystallization at 800°C with 100 ppm O_2 in N_2 atmosphere with or without an intermediate dwelling step following by an annealing step at 450°C for 2 hours under pure O_2 atmosphere.[13] Their average (inductive) self-field critical current densities at 77 K are given in Table 1. These samples for inductive measurements came out of used typically good samples with high reproducibility and disregarded only obviously erroneous samples when some mistake during deposition process was spotted. The intermediate step at 650°C clearly results in an improved J_c of 5.5 ± 0.20 MA/cm^2 for undoped YBCO (average of six samples) and 5.80 ± 0.21 MA/cm^2 for ZrO_2-doped YBCO (six samples) compared to J_c values of both precursors without an intermediate dwelling step. This is also confirmed via XRD patterns (Figure 3B), indicating that the thermal process with the additional dwelling step of

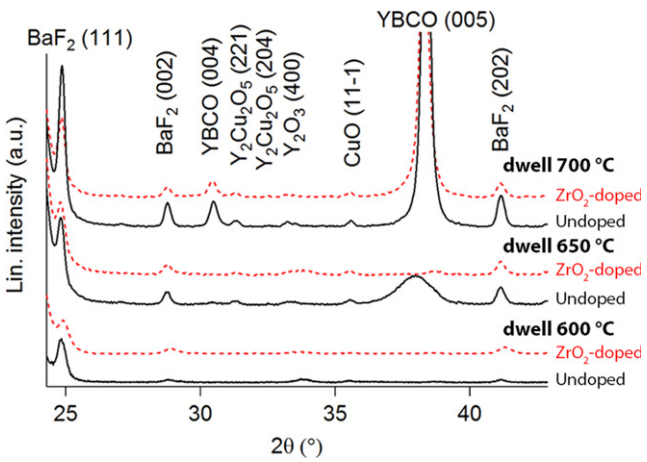

FIGURE 2 X ray diffraction patterns of undoped (black, full line) and ZrO_2 doped (red, dotted line) YBCO samples quenched after dwelling at 600, 650, and 700°C. YBCO, $YBa_2Cu_3O_{7-\delta}$ [Color figure can be viewed at wileyonlinelibrary.com]

undoped YBCO layers increases the formation of Y_2O_3 (222) ($2\theta = 29.2°$) and the reduces $Ba_xCu_yO_z$ ($2\theta = 27.7°$) amount. The formation of the $Ba_xCu_yO_z$ phase is also prevented by the introduction of ZrO_2 nanocrystals in combination with the increase of Y_2O_3 (222) which can contribute to pinning.[17] So, the additional dwelling step at 650°C reduces undesired secondary phases in the YBCO matrix of the nanocomposite film and thus improves the YBCO morphology compared to undoped YBCO layer. This presumption is verified by SEM images of undoped and ZrO_2-doped layers after the thermal process with additional dwelling step (Figure S2). Notwithstanding an extra advantage of the improvement in YBCO texture with minor secondary phases, the introduction of an additional dwelling step does not minimize the particle growth in contradiction with results often reported in the literature. The size distribution of $BaZrO_3$ particles (determined and fitted via two different cross-sectional HAADF-STEM images of nanocomposites, Figure S5) shows a mean diameter of 14.2 ± 5.2 nm after the thermal process without the intermediate dwelling step. Thus, the preformed ZrO_2 nanocrystals with 3-4 nm diameter have coarsened by four times to $BaZrO_3$ particles during the thermal process due to their reactivity with the Ba-containing intermediate products and probably also due to minor effects of agglomeration.

By lowering the temperature of the intermediate step to 600°C, T_c decreases for both precursors but undoped YBCO still shows a fairly low J_c of 0.61 MA/cm^2 while ZrO_2-doped YBCO did not show a finite J_c due to the bad epitaxial structure (eg, low *c*-oriented YBCO reflections in Figure S3). The reduced J_c values of undoped YBCO films after thermal processing with an additional dwelling step at 600°C is due to the presence of $Ba(O,F_2)$ in the YBCO layer as confirmed by XRD (Figure S3) $2\theta = 24.9(111)$, 28.9(002), and 41.2(202) which indicates that the YBCO formation is incomplete. When increasing the temperature of the intermediate dwelling step to 700°C, more secondary phases and *a*/*b*-oriented YBCO grains (needle shaped structure in SEM image, Figure S4) are formed which would degrade the superconducting properties. At this temperature of 700°C, the *a*/*b*-oriented YBCO grains are preferred over *c*-oriented YBCO grains, leading to a needle shaped structure on top of the YBCO layer (Figure S4). This is due to the faster growth of *a*/*b*-grains along the (100)/(010) plane. So, this means that the introduction of an intermediate dwelling step in the range of 640 650°C does not improve the distribution of nanoparticles in the YBCO matrix but results in the improvement in the superconducting properties of the YBCO matrix itself. We can therefore conclude that the temperature of the intermediate dwelling step is very crucial to obtain an enhancement of J_c for both undoped and ZrO_2-doped YBCO films. This enhancement via introduction of the additional dwelling step may be

TABLE 1 Average self field critical current density J_c at 77 K of six samples, critical temperature T_c and width of the transition temperature of undoped $YBa_2Cu_3O_{7-\delta}$ (YBCO) and ZrO_2 doped YBCO layer after the complete thermal process with an additional dwell step at different temperatures

	Undoped YBCO			ZrO_2-doped YBCO		
Dwell temperature (°C)	J_c (MA/cm²)	T_c (K)	ΔT_c (K)	J_c (MA/cm²)	T_c (K)	ΔT_c (K)
700	1.25 ± 0.23	90.1	0.4	1.10 ± 0.25	91.1	0.4
650	5.51 ± 0.20	91.4	0.6	5.80 ± 0.21	91.6	0.9
600	0.61 ± 0.26	89.2	0.5	0.00 ± 0.00	89.1	1.3
No dwell	2.52 ± 0.35	90.6	0.7	2.39 ± 0.32	90.9	0.7

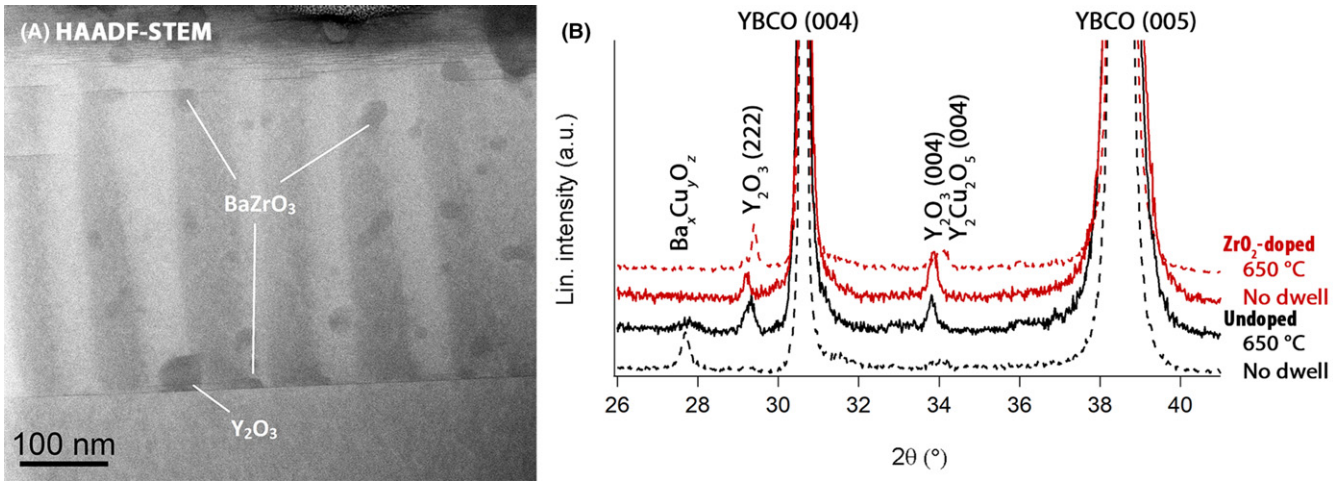

FIGURE 3 A, HAADF STEM image of ZrO_2 doped $YBa_2Cu_3O_{7-\delta}$ (YBCO) after thermal process without a dwell step. $BaZrO_3$ particles (indicated via phase analysis) are randomly distributed in the YBCO matrix. B, X ray diffraction patterns of undoped and ZrO_2 doped YBCO layer after thermal process with or without a dwell step [Color figure can be viewed at wileyonlinelibrary.com]

compared to pulsed laser deposition-grown samples where the nuclei density can be controlled by deposition temperature,[31] laser frequency,[32] or nano-crystallinity of the target.[33] It is mentioned in literature[34–36] that, for CSD-based materials, the intermediate dwelling step prevents accumulation of particles at the $LaAlO_3$ interface and hence excessive grain growth and also minimizes agglomeration of nanocrystals in YBCO matrix. However, we observe in this study that, even during thermal processing without the intermediate dwelling step, an accumulation of nanocrystals at the $LaAlO_3$ interface did not occur, as confirmed by HAADF-STEM image (Figure 3) and TOF-SIMS analysis (Figure S1B,C).

To determine the improvement in vortex pinning, the magnetic field dependence of the transport critical current densities at 77 K and magnetic field (B) parallel to c-axis of YBCO ($B||c$) of an undoped and a ZrO_2-doped YBCO film (good selected samples from Table 1) was shown on Figure 4. This indicates that the addition of ZrO_2 nanocrystals has enhanced the capabilities to pin the vortices. The use of the additional dwelling step (red data) results in a higher maximum pinning force density F_p^{max} of around 7.3 GN/m^3 at 0.8 T for the ZrO_2-doped and around 2.5 GN/m^3 at 1.5 T for the undoped film, while the absence of the additional dwell step (black data) results in F_p^{max} of 6.0 GN/m^3 at 0.9 T for the ZrO_2-doped and 2.1 GN/m^3 at 1.3 T for the undoped film. Thus, clearly the addition of 5 mol-% ZrO_2 nanocrystals in the YBCO matrix increases F_p^{max} by a factor of three while the introduction of an additional dwelling step further increases self-field and in-field J_c and does not minimize or prevent the coarsening of the nanocrystals during the thermal process resulting in a further increase in in-field performance and maximum F_p. But it is remarkable that the maximum of F_p is shifted toward lower magnetic fields by the addition of nanocrystals. Based on F_p curves of the undoped and ZrO_2-doped films, it seems that ZrO_2-doped YBCO shows a better pinning performance at low magnetic field compared to undoped YBCO films due to the contribution of the nanocrystals with a certain particle size and density.[37] The shift of F_p^{max} from 1.3 T for undoped YBCO without additional dwelling step to 1.5 T for undoped

YBCO with additional dwelling step is explained as follows: Y_2O_3 particles naturally grown during thermal process are more present in undoped YBCO layers without an additional dwelling step as observed in XRD (Figure 3B), and as Y_2O_3 particles can contribute to the pinning performance. So, the addition of preformed nanocrystals or the introduction of self-assembled nanoparticles can lead to a shift of maximum F_p value toward a lower magnetic field. A follow-up study should be essential to understand the origination of this shifting effect.

The additional dwelling step in this work does not contribute to the tuning of final particle size in YBCO matrix. It is in contrast to already published results where an additional intermediate dwell step at lower temperatures before the YBCO crystallization was introduced to offer the opportunity to tune the particle size during the self-assembled growth of randomly oriented nanoparticles.[34–36] The F_p^{max} values of ZrO_2-doped YBCO films after the introduction of the intermediate dwelling step are larger than a 12 mol-% self-assembled $BaHfO_3$-YBCO film (F_p^{max} = 4 GN/m^3 at 1.2 T)[38] and 10 mol-% self-assembled Ba_2YTaO_6 YBCO film (F_p^{max} = 6 GN/m^3 at ~1 T)[39] yet slightly lower than the champion value (F_p^{max} = 22 GN/m^3) reported on a self-assembled $BaZrO_3$ YBCO nanocomposite film[16] and self-assembled $BaHfO_3$ $GdBa_2Cu_3O_{7-\delta}$ film (F_p^{max} = 16 GN/m^3 at 2 T).[40] Nonetheless, F_p^{max} values of 7.3 GN/m^3 are highest for CSD-based YBCO nanocomposite films starting with preformed nanocrystals compared to 5 mol-% ZrO_2-doped LF-YBCO films (F_p^{max} = 5.5 GN/m^3)[17] and 10 mol-% ZrO_2-doped TFA-YBCO films (F_p^{max} = 6 GN/m^3).[18] This means that the combination of preformed nanocrystals and intermediate dwelling step leads to an increase of superconducting properties, while the addition of preformed nanocrystals leads to a shift of F_p^{max} toward lower magnetic fields. This intermediate dwelling step at 650°C during thermal process is also applicable to films on (100) $SrTiO_3$ substrate as it results in high self-field J_c values of >4.5 MA/cm^2 at 77 K for undoped and ZrO_2-doped YBCO films. The ZrO_2-doped YBCO film on $SrTiO_3$ substrate shows also better pinning properties (eg, a slower decay of J_c with magnetic field) compared to undoped YBCO films (see Figure S6).

The next topic to investigate for this CSD method is to improve the self-field J_c at 77 K of YBCO nanocomposite films in combination with increased thickness, because the YBCO growth gets more and more disturbed for increased thickness of the pyrolyzed layer resulting in nonideal microstructure, for example, increasing *a* axis content[41] and pore formation and therefore reduced J_c values.[42] Furthermore, for an essential breakthrough to commercial production, these results have to be transferred to textured Ni W tape with an epitaxial oxide buffer system or polycrystalline Hastelloy tape with a complex sequence of oriented oxide buffer layers.[1] Both types of technical tape have an additional CeO_2 cap layer. This transfer is challenging because the YBCO growth rate on an oxide buffer layer is different from growth on single crystal substrates due to less well-defined (00ℓ) terminations of the CeO_2 oxide layer and the increased surface roughness which will affect the YBCO nuclei density.[43] This limitations can be obviated by the optimization of growth rate, temperature, and duration of the additional dwelling step during the thermal process which is the focus of future studies.

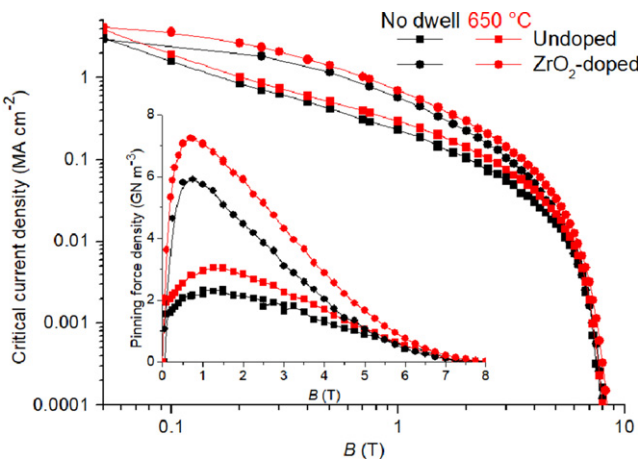

FIGURE 4 Magnetic field dependence of the transport J_c showing the in field enhancement of J_c by both the addition of ZrO_2 nanocrystals to the solution (symbol) and/or of a dwelling step at 650°C in the heat treatment (color) [Color figure can be viewed at wileyonlinelibrary.com]

4 CONCLUSION

In summary, we have proven that the addition of preformed ZrO_2 nanocrystals results in a delay rather than in a degradation in YBCO nucleation and growth due to the Ba^{2+} consumption of nanocrystal between temperatures of 600 and 700°C, leading to the formation of $BaZrO_3$ particles. Therefore, an additional dwelling step was introduced to form a higher content of the (002)-oriented BaF_2 superstructure which acts as a template for YBCO nucleation. This intermediate dwelling step improved the YBCO texture and led to the reduction of secondary phases rather than it altered the distribution as well as the miniaturization of nanocrystals in the YBCO matrix, which is often described in literature. This CSD approach with additional dwelling step thereby showed the improved texture and structure purity, leading to highly reproducible undoped YBCO films with good superconducting properties of 5.5 MA/cm^2. Combining with the addition of preformed ZrO_2 nanocrystals resulted in a J_c of 5.8 MA/cm^2. The insights developed in this work will contribute to further

research and development of YBCO nanocomposite films on technical substrates.

ACKNOWLEDGMENTS

The authors want to thank M. Van Zele (Ghent University) for TOF-SIMS analysis, Dr. J. Bennewitz (BASF SE) for XRD and Cryoscan measurements and R. Nast (KIT) for structuring of nanobrigdes. This work was financially supported by the European Union Horizon 2020 Marie Curie Actions under the project SynFoNY (H2020/2016-722071).

REFERENCES

1. Obradors X, Puig T. Coated conductors for power applications: materials challenges. Supercond Sci Technol. 2014;27(4):044003.
2. Larbalestier D, Gurevich A, Feldmann DM, Polyanskii A. High T_c superconducting materials for electric power applications. Nature. 2001;414(6861):368 77.
3. Pahlke P, Sieger M, Ottolinger R, Lao M, Eisterer M, Meledin A, et al. Influence of artificial pinning centers on structural and superconducting properties of thick YBCO films on ABAD YSZ templates. Supercond Sci Technol. 2018;31(4):044007.
4. Selvamanickam V, Gharahcheshmeh MH, Xu A, Zhang Y, Galstyan E. Critical current density above 15 MA cm^{-2} at 30 K, 3 T in 2.2 μm thick heavily doped $(Gd,Y)Ba_2Cu_3O_x$ superconductor tapes. Supercond Sci Technol. 2015;28(7):072002.
5. Obradors X, Puig T, Pomar A, Sandiumenge F, Pinol S, Mestres N, et al. Chemical solution deposition: a path towards low cost coated conductors. Supercond Sci Technol. 2004;17(8):1055.
6. Pollefeyt G, Clerick S, Vermeir P, Feys J, Hühne R, Lommens P, et al. Ink jet printing of SrTiO3 buffer layers from aqueous solutions. Supercond Sci Technol. 2014;27(9):095007.
7. Van Driessche I, Feys J, Hopkins SC, Lommens P, Granados X, Glowacki BA, et al. Chemical solution deposition using ink jet printing for YBCO coated conductors. Supercond Sci Technol. 2012;25(6):065017.
8. De Keukeleere K, Pollefeyt G, Feys J, De Roo J, Rijckaert H, Lommens P, et al. Chemical solution deposition of functional ceramic coatings using ink jet printing. Pure Appl Chem. 2015;87(3):231 8.
9. Araki T, Hirabayashi I. Review of a chemical approach to $YBa_2Cu_3O_{7-x}$ coated superconductors metalorganic deposition using trifluoroacetates. Supercond Sci Technol. 2003;16(11):R71 94.
10. Solovyov V, Dimitrov IK, Li Q. Growth of thick YBa2Cu3O7 layers via a barium fluoride process. Supercond Sci Technol. 2012;26(1):013001.
11. Palmer X, Pop C, Eloussifi H, Villarejo B, Roura P, Farjas J, et al. Solution design for low fluorine trifluoroacetate route to $YBa_2Cu_3O_7$ films. Supercond Sci Technol. 2016;29(2):024002.
12. Chen Y, Wu C, Zhao G, You C. An advanced low fluorine solution route for fabrication of high performance YBCO superconducting films. Supercond Sci Technol. 2012;25(6):062001.
13. Rijckaert H, De Roo J, Roeleveld K, Pollefeyt G, Bennewitz J, Bäcker M, et al. Microwave assisted $YBa_2Cu_3O_7$ precursors: a fast and reliable method towards chemical precursors for superconducting films. J Am Ceram Soc. 2016;100(6):2407 18.
14. Vermeir P, Cardinael I, Bäcker M, Schaubroeck J, Schacht E, Hoste S, et al. Fluorine free water based sol gel deposition of highly epitaxial $YBa_2Cu_3O_{7-\delta}$ films. Supercond Sci Technol. 2009;22(7):075009.
15. MacManus Driscoll J, Foltyn S, Jia Q, Wang H, Serquis A, Civale L, et al. Strongly enhanced current densities in superconducting coated conductors of $YBa_2Cu_3O_{7\ x}$+$BaZrO_3$. Nat Mater. 2004;3(7):439 43.
16. Gutierrez J, Llordes A, Gazquez J, Gibert M, Roma N, Ricart S, et al. Strong isotropic flux pinning in solution derived $YBa_2Cu_3O_{7-x}$ nanocomposite superconductor films. Nat Mater. 2007;6(5):367 73.
17. Rijckaert H, Pollefeyt G, Sieger M, Hänisch J, Bennewitz J, De Keukeleere K, et al. Optimizing nanocomposites through nanocrystal surface chemistry: superconducting $YBa_2Cu_3O_7$ thin films via low fluorine metal organic deposition and preformed metal oxide nanocrystals. Chem Mater. 2017;29(14):6104 13.
18. De Keukeleere K, Cayado P, Meledin A, Vallès F, De Roo J, Rijckaert H, et al. Superconducting $YBa_2Cu_3O_{7\ \delta}$ nanocomposites using preformed ZrO_2 nanocrystals: growth mechanisms and vortex pinning properties. Adv Electron Mater. 2016;2(10):1600161.
19. Rijckaert H, De Roo J, Van Zele M, Banerjee S, Huhtinen H, Paturi P, et al. Pair distribution function analysis of ZrO_2 nanocrystals and insights in the formation of ZrO_2 $YBa_2Cu_3O_7$ nanocomposites. Materials. 2018;11(7):1066.
20. Malmivirta M, Rijckaert H, Paasonen V, Huhtinen H, Hynninen T, Jha R, et al. Enhanced flux pinning in YBCO multilayer films with BCO nanodots and segmented BZO nanorods. Sci Rep. 2017;7(1):14682.
21. Sieger M, Pahlke P, Hänisch J, Sparing M, Bianchetti M, MacManus Driscoll J, et al. $Ba_2Y(Nb/Ta)O_6$ doped YBCO films on biaxially textured Ni 5at.% W substrates. IEEE Trans Appl Supercond. 2016;26(3):1 5.
22. Hänisch J, Cai C, Stehr V, Hühne R, Lyubina J, Nenkov K, et al. Formation and pinning properties of growth controlled nanoscale precipitates in $YBa_2Cu_3O_{7-\delta}$/transition metal quasi multilayers. Supercond Sci Technol. 2006;19(6):534 40.
23. De Keukeleere K, Coucke S, De Canck E, Van Der Voort P, Delpech F, Coppel Y, et al. Stabilization of colloidal Ti, Zr, and Hf oxide nanocrystals by protonated tri n octylphosphine oxide (TOPO) and its decomposition products. Chem Mater. 2017;29(23):10233 42.
24. De Roo J, Coucke S, Rijckaert H, De Keukeleere K, Sinnaeve D, Hens Z, et al. Amino acid based stabilization of oxide nanocrystals in polar media: from insight in ligand exchange to solution ^1H NMR probing of short chained adsorbates. Langmuir. 2016;32(8):1962 70.
25. Zalamova K, Pomar A, Palau A, Puig T, Obradors X. Intermediate phase evolution in YBCO thin films grown by the TFA process. Supercond Sci Technol. 2009;23(1):014012.
26. Jin LH, Lu YF, Feng JQ, Zhang SN, Yu ZM, Wang Y, et al. Evolution of low fluorine solution in decomposition and crystallization for $YBa_2Cu_3O_y$ film growth. J Alloy Compd. 2013;568:36 41.

27. Wesolowski D, Yoshizumi M, Cima M. Understanding the MOD process between decomposition and YBCO formation. IEEE Trans Appl Supercond. 2007;17(2):3351 4.
28. Jin L, Li C, Feng J, Yu Z, Wang Y, Lei L, et al. Optimization of fluorine content in TFA MOD precursor solutions for YBCO film growth. Supercond Sci Technol. 2015;29(1):015001.
29. Gazquez J, Sandiumenge F, Coll M, Pomar A, Mestres N, Puig T, et al. Precursor evolution and nucleation mechanism of $YBa_2Cu_3O_x$ films by TFA metal organic decomposition. Chem Mater. 2006;18(26):6211 9.
30. Cayado P, De Keukeleere K, Garzón A, Perez Mirabet L, Meledin A, De Roo J, et al. Epitaxial $YBa_2Cu_3O_{7-x}$ nanocomposite thin films from colloidal solutions. Supercond Sci Technol. 2015;28(12):124007.
31. Feldmann D, Ugurlu O, Maiorov B, Stan L, Holesinger T, Civale L, et al. Influence of growth temperature on critical current and magnetic flux pinning structures in $YBa_2Cu_3O_{7-x}$. Appl Phys Lett. 2007;91(16):162501.
32. Golovchanskiy IA, Pan AV, Fedoseev SA, Higgins M. Significant tunability of thin film functionalities enabled by manipulating magnetic and structural nano domains. Appl Surf Sci. 2014;311:549 57.
33. Paturi P, Huhtinen H, Laajalehto K, Laiho R. Reason for high critical current in thin YBCO films prepared by laser ablation from nanostructured target. Supercond Sci Technol. 2000;13(5):622.
34. Nakaoka K, Yoshida R, Kimura K, Kato T, Usui Y, Izumi T, et al. Another approach for controlling size and distribution of nanoparticles in coated conductors fabricated by the TFA MOD method. Supercond Sci Technol. 2017;30(5):055008.
35. Coll M, Guzman R, Garcés P, Gazquez J, Rouco V, Palau A, et al. Size controlled spontaneously segregated Ba_2YTaO_6 nanoparticles in $YBa_2Cu_3O_7$ nanocomposites obtained by chemical solution deposition. Supercond Sci Technol. 2014;27(4):044008.
36. Horita H, Teranishi R, Yamada K, Kaneko K, Sato Y, Otaguro K, et al. Miniaturization of $BaHfO_3$ nanoparticles in $YBa_2Cu_3O_y$ coated conductors using a two step heating process in the TFA MOD method. Supercond Sci Technol. 2016;30(2):025022.
37. Paturi P, Malmivirta M, Palonen H, Huhtinen H. Dopant diameter dependence of J(c)(B) in doped YBCO films. IEEE Trans Appl Supercond. 2016;26(3):8000705.
38. Erbe M, Hänisch J, Hühne R, Freudenberg T, Kirchner A, Molina Luna L, et al. $BaHfO_3$ artificial pinning centres in TFA MOD derived YBCO and GdBCO thin films. Supercond Sci Technol. 2015;28(11):114002.
39. Coll M, Ye S, Rouco V, Palau A, Guzman R, Gazquez J, et al. Solution derived $YBa_2Cu_3O_7$ nanocomposite films with a Ba2Y TaO6 secondary phase for improved superconducting properties. Supercond Sci Technol. 2012;26(1):015001.
40. Cayado P, Mundet B, Eloussifi H, Valles F, Bau MC, Ricart S, et al. Epitaxial superconducting $GdBa_2Cu_3O_{7\ d}/Gd_2O_3$ nanocomposite thin films from advanced low fluorine solutions. Supercond Sci Technol. 2017;30:125010.
41. Boubeche M, Cai C, Jian H, Li M, Yang W, Liu Z, et al. Thick REBaCuO superconducting films through single coating of low fluorine metallorganic solution. Cryogenics. 2016;79:49 52.
42. Kim S, Gurevich A, Song X, Li X, Zhang W, Kodenkandath T, et al. Mechanisms of weak thickness dependence of the critical current density in strong pinning ex situ metal organic deposition route $YBa_2Cu_3O_{7\ x}$ coated conductors. Supercond Sci Technol. 2006;19(9):968.
43. Solovyov VF, Develos Bagarinao K, Li Q, Qing J, Zhou J. Nature of Y1Ba2Cu3O7 nucleation centers on ceria buffers. Supercond Sci Technol. 2009;23(1):014008.

SUPPORTING INFORMATION

Additional supporting information may be found online in the Supporting Information section at the end of the article.